

Technology Maturation for Multi-Gigabit/sec Optical Communications Transceiver for Earth Science

Gerry G. Ortiz, Shinhak Lee and Hamid Hemmati

Jet Propulsion Laboratory
California Institute of Technology
Pasadena, CA 91109

Abstract—Optical communication technologies are being developed to support multi-gigabit/sec links that encompass the LEO-to-GEO and GEO-to-GROUND communication system. One area of focus has been in demonstrating the applicability and availability of high (up to 10 Gbps) data-rate receive/transmit components. A 7.5 Gbps link was demonstrated in the laboratory, matching to within 2 dB the analytically predicted performance.

A second area of research is the development and risk mitigation of an ATP subsystem that enables optical communication links with data rates up to 10 Gbps. Specifics of this research include mission scenarios, basic architectures, functional and performance requirements, system design trades, risk analysis and mitigation plans. Innovative concepts being investigated are 1) reducing the tracking loss duration and probability by the use of inertial sensors in the tracking control loop; 2) a design that eliminates the need for a search sequence (or a re-acquisition sequence); 3) single beacon divergence/laser; 4) reduced ephemeris update rate; 5) miniaturization of ATP subsystem and an 6) all optical system. The potential benefits of these innovations are longer duration links, increased data volume throughput, improved BER (at Gbps data rates), simpler design, robust acquisition/tracking handover, reduced size, weight and power, single ground station for telemetry and data, and no RF comm required to enable optical comm. This research task is also mitigating risk through a laboratory demonstration of the ATP subsystem. To this end two ATP terminals (a LEO and a GEO) have been designed and are currently being assembled. The laboratory experiment will demonstrate the ATP subsystem functionality and performance while the terminals undergo simulated spacecraft vibrations, orbital motions, and spacecraft attitude uncertainties.

I. INTRODUCTION

In order to address the anticipated need to deliver to the scientists, the expected enormous volumes of data gathered by remote sensing spacecraft, this task has been developing high rate optical communication technologies for LEO-to-GEO and GEO-to Ground links. The effort has focused in the design, development and demonstration of the two key subsystems: 1) the high rate communication subsystem (up to 10 Gbps), and 2) the acquisition, tracking and pointing subsystem. The high rate subsystem was the major thrust in FY01. This year the thrust has been on the ATP subsystem. This paper will discuss the maturation of the two subsystems but with a major emphasis on the ATP work's

current accomplishments and details of the planned efforts for the remaining of the fiscal year.

II. HIGH RATE COMMUNICATIONS

As part of this task a free space optical communication link at a data rate of 5.4 Gbps with BER better than $10E-9$ was demonstrated in the laboratory [1]. Three separate fiber coupled laser sources were combined in a single transmitter and then wavelength division de-multiplexed through free space optics at the receiver. The three independent channels incorporated a 2.5 Gbps PRBS signal, a 1.5 Gbps uncompressed HDTV signal and a 1.4 Gbps BER test signal. The data rate demonstration was limited by the available test equipment and could support a data rate of 7.5 Gbps with the current optics. Bit error rates of better than $10E-9$ were measured with no cross talk or channel interference visible in the received signal. A fiber amplifier coupled through a 10 cm transmit telescope to a 30 cm receive telescope is also available to propagate the three channels with a total signal output power of 2 W around a wavelength of 1550 nm. A link range of greater than 1000 km can be satisfied with the current components and sufficient margin. The system is designed as a proof of concept for inter-satellite links with the eventual goal of demonstrating a LEO to GEO optical link.

III. ATP SYSTEM ENGINEERING

The goal of the system engineering task has been to identify the requirements, analyze what it takes to meet them, and mitigate major risks through laboratory demonstrations. The overall communications link design and budget was presented in [1]. In summary the transceiver system for Multi-Gigabit/sec Earth Science applications uses a 1550 nm transmit wavelength, typical link ranges of 4.3E4 km, bit error rates of $1E-7$, transmit aperture of 30 cm and receive aperture of 30 cm with a 3 dB link margin. The ATP Subsystem was allocated a 2 dB pointing loss with a 0.03% pointing fade probability.

A. Mission Scenario

The typical mission scenario is depicted in Figure 1 where the GEO satellite is at 40,000 km and LEO satellite is at 400 km. The LEO orbit can be co-planar and some communication outage is expected in that case. The time of

operation is determined by the ground station control. The GEO terminal initiates by scanning its beacon beam over its attitude uncertainty cone looking for LEO while LEO terminal is sampling to receive it while in a stare mode. Once the LEO terminal acquires the beacon beam, then the LEO terminal tracks and acknowledges by transmitting the data beam towards the GEO terminal. At this point the GEO stops searching and locks on to the beam from the LEO terminal. Tight pointing is maintained during the communication link. The pointing requirement is set by the communication link budget. From the 2 dB allocated (with 0.03% fade probability) a jitter and a bias pointing error can be derived.

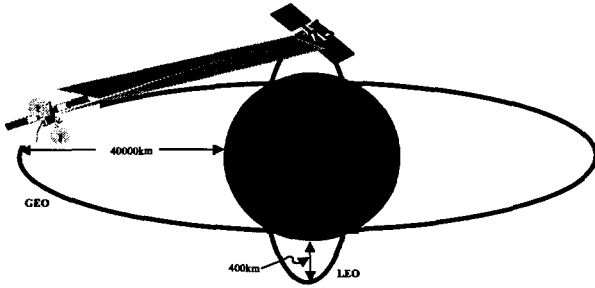


Fig. 1. Multi-gigabit optical communications link.

B. S/C Attitude Control Uncertainty

Spacecraft (S/C) attitude control uncertainty affects the design of the camera, particularly, the acquisition FOV for optical comm. If there is no attitude control error, then the camera FOV would be driven only by scientific and operational needs. However, because of this error, the final FOV needs to be larger by the attitude control uncertainty. At the same time, we do not want to make it too large since it will increase background noise. To determine the attitude control uncertainty of the S/C that will carry the optical comm terminal in LEO and GEO orbit, we surveyed 28 Earth orbiting satellites (LEO, GEO, FTO, HEO). Figure 2, shows that the majority (15 out of 28) of S/C attitude control uncertainty's fall within ± 2 mrad (3σ). Between 2 and 5 mrad, there is only one sample point (3.4 mrad). There are 5 and 7 sample points, respectively, for between 5-10 mrad, and between 10-90 mrad. In Table 1, we list the average attitude control uncertainty based on S/C launch mass. This is motivated by the strong correlation existing between those two parameters which indicates that overall attitude control uncertainty is inverse proportional to the launch mass. This statement is not true for all cases since some S/C might allocate major mass to scientific instrument (thus poor attitude control) and some small S/C might allocate most mass to attitude control instruments, thereby achieving a good attitude control. Table I reconfirms this correlation again, except for the cases of 200-500 kg S/C and more than 2000 kg. But even for these cases, the average numbers become to more reasonable number of

11.33 mrad and 0.38, if we take out one very large 'outlier' number (85 mrad and 5.1 mrad) from the rest of the groups. This anomaly is due to lack of sample points in this study. In conclusion we can see that 2 mrad attitude control uncertainty covers the majority of S/C's. Table I shows the average of 4 mrad attitude control uncertainty from majority S/C's of launch mass 500 kg or more. Without any specific S/C details, 4 mrad attitude control uncertainty, that represents majority S/C's, seems to be a compelling design number. At the same time, we need to be aware of the assumed S/C launch mass of 500 kg or more.

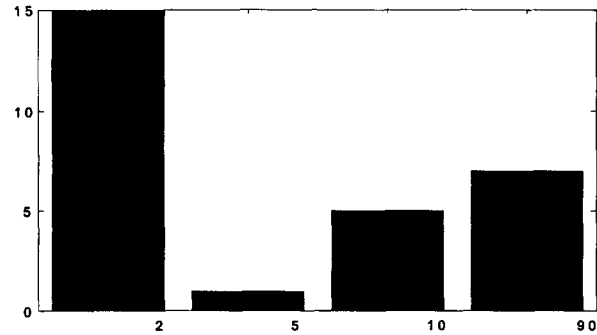


Fig. 2. Histogram of s/c attitude control uncertainty (mrad, 3σ).

Table I. S/C mass vs. attitude control uncertainty.

S/C Mass	Avg. Attitude control uncertainty (mrad)
Below 100Kg	46.75
100-200Kg	19.98
200-500Kg	29.75 (11.33)
500-1000Kg	3.77
1000-2000Kg	0.73
More than 2000Kg	1.33 (0.38)

C. S/C Vibration

S/C vibration is the major source of pointing error. Without compensating for it or isolating it, the optical comm terminal cannot achieve accurate and stable links. In order to design the ATP subsystem, the S/C vibration PSD (as a function of frequency) for the unknown future S/C that will carry our optical comm terminal needs to be baselined. Figure 3 shows a sample of various S/C vibration PSD's. Some are converted from linear acceleration measurements to angular vibrations PSD (urad^2/Hz), some are direct measurements of angular vibrations, and the others are specifications as published. As shown, the magnitude of spectral contents vary as much as 10^6 to 10^8 (between shuttle and Astro-Spas). Just like attitude control uncertainty, S/C vibration depends on many parameters such as the type of S/C and onboard instruments (especially moving instrument such as thrusters, reaction wheels, and etc.). Except for Iridium, most S/Cs exhibit common

characteristics of attenuation in vibration magnitude as frequency increases.

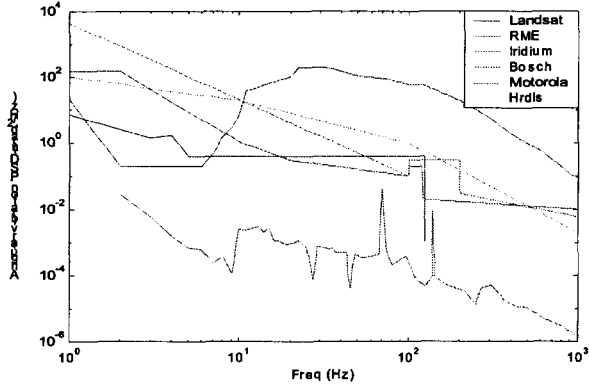


Fig. 3. Various spacecraft angular vibration PSD's.

Eleven (11) S/C's were surveyed and grouped into three classes: Very quiet S/Cs, Average S/Cs, and Noisy S/Cs (shown in Table II with red lines). Without much investigation, it is clear that very quiet S/Cs have reasons to be very quiet. For example, RME minimizes eliminated vibration from solar panel by attaching solar panel to the S/C surface (instead of expandable solar panel) – no moving parts!

S/C name	S/C RMS Disturbance (urad)			
	(1-10Hz)	(10-100Hz)	(100-1kHz)	(1~1kHz)
ASTRO-SPAS	0.58	0.45	0	0.59
STRV-2	0.22	0.03	0.02	0.22
RME	0.10	0.35	0.17	0.40
CASSINI	1.33	1.48	0.01	1.92
Olympus	7.76	4.01	1.20	11.49
Motorola	17.56	4.43	3.93	18.49
Landsat	3.42	6.07	3.21	7.62
Bosch	61.70	13.18	6.29	63.22
Hrdls	18.37	18.79	7.66	26.97
Iridium	4.52	99.19	76.34	124.99
Shuttle	219.65	477.95	15.15	519.29

Table II. RMS S/C vibration in various frequency bands.

For the noisier S/C's for which vibrations cannot be mitigated by compensation techniques (optical tracking, feed-forward), there are two options to reduce their impact on the beam pointing. These are passive and/or active isolation. Passive isolation uses simple devices such as artificially made silicone to dampen high frequency. Active isolation utilizes vibration sensors and actuators to dampen both low and high frequency vibrations. Gains from using passive isolators are from 10 % to 30 % reduction in

residual tracking error. Active isolators, on the other hand, can give as much as 20 dB isolation, depending on the spectral content, which translates to 1/10th of the residual tracking error. For the preliminary design of the ATP subsystem, it may be appropriate to avoid extreme S/C (either very quiet or very noisy). We can mitigate some of the higher vibration using passive and active isolators and reduce the residual tracking error by up to 90%. Even so, some of S/Cs such as shuttle and Iridium seem to be prohibitive as an optical comm ATP carrier. As a median S/C in terms of vibration, Olympus S/C still seems to represent good model for our preliminary design. Landsat is also a good baseline, especially with passive and active isolation strategies on hand.

IV. ATP SUBSYSTEM DESIGN AND ANALYSIS

A. Pointing Error Allocation

In order to design ATP subsystem, we need to determine what performance each component must have, to meet the pointing requirement while compensating for spacecraft vibrations and s/c attitude uncertainty. To meet the 2 dB pointing loss allocated from the link power budget with a 0.03 % fade probability means that the ATP subsystem must have a total pointing accuracy of 2 urad, 3 sigma. This total pointing is divided into a jitter and a bias component. The following table shows just the jitter portion. The static error allocation (0.5 urad) will be discussed later. The design process begins by creating a pointing budget that is then verified through simulations of the different components. The allocation process starts with the parameters of the sensor or the signal at similar levels of technical feasibility. Table III lists the pointing jitter budget where each component is at least at a technology readiness level (TRL) of 4 or higher.

B. Noise Equivalent Angle

Equation for the random centroid error (or NEA, noise equivalent angle) from [2] is summarized here:

$$NEA = \sqrt{(S + N_p(\text{Var}(R_f) + \Delta t R_T)/S^2)N(N + 1)/3} \quad (1)$$

where S = total signal,
 Δt = the exposure time,
 N = Truncated half width of centroiding area,
 N_p = Number of pixels involved in the centroiding area, $N_p = (2N+1)^2$
 R_f = Fixed per pixel noise (1σ), such as read noise,
 R_T = Per pixel background signal (including straylight and dark current),

Eq.(1) indicates that NEA is inversely proportional to SNR. Therefore, either the signal needs to be increased or the noise needs to be decreased in order to reduce the NEA. This implies that the effect of the noise is small if the signal is relatively larger than the noise and vice versa. Using the parameters in the above table, the resulting NEA is 0.16 urad.

Errors	Sources	Value	RMS Pointing Error (urad)
BEACON NEA	FPA read noise/pixel (e-)	100	0.16
	# of ADC bits	8	
	FPA full well (e-)	30000	
	Total signal (e-)	100000	
	Centroid window (pixels)	7	
	FPA pixel FOV (urad)	10	
	Spot size (pixel)	5	
Spatial quantization	Beam type	Airy	0.02
Pixel Non-uniformity	Maximum pixel non-uniformity (%)	5	0.08
TRANSMIT BEAM NEA	FPA read noise/pixel (e-)	100	0.16
	# of ADC bits	8	
	FPA full well (e-)	30000	
	Total signal (e-)	100000	
	Centroid window (pixels)	7	
	FPA pixel FOV (urad)	10	
	Spot size (pixel)	5	
Spatial quantization	Beam type	Airy	0.02
Pixel Non-uniformity	Maximum pixel non-uniformity (%)	5	0.08
Residual tracking error	Disturbance rejection freq. Response	Update rate	0.34
	S/C vibration PSD	Olympus	
Gimbal vibration	Measured vibration at the interface		0.24
Total pointing jitter (1sigma)			0.50

Table III. ATP Subsystem Pointing Jitter Budget

C. Pixel Non-uniformity

Pixel non-uniformity is a property of the individual pixel response, hence does not change over short period of time. The effects on centroid error appear to be a slowly changing bias as an beacon image moves across a pixel. There are two cases to consider: a) high background signal and b) low background signal.

a) High background signal: Examples include straylight and Earth image. This can be treated in a RMS sense; if the (uncalibrated) RMS non-uniformity value is σ_U , and the background rate signal is R_T electrons per pixel, then the RMS noise variance is $(\sigma_U \Delta t \times R_T)^2$ per pixel for an integration time of Δt . This is treated for simplicity as if it were a read noise term.

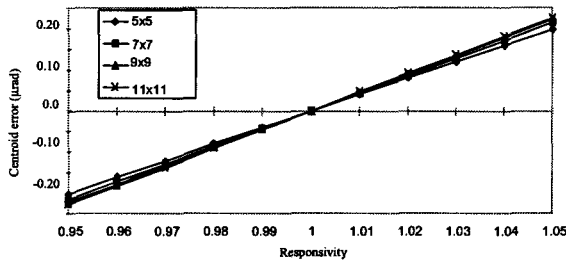


Fig. 4. Centroid error due to non-uniformity of FPA columns.

b) Low background signal: Only the beacon image is of importance in this case. The simulation results in Figure 4 assume the worst-case scenario where only the right most column of the centroiding window has different responsivity than the other columns (which here have responsivity of 1). Figure 4 shows the corresponding centroid error given various non-uniformity from 0 to

5%. For the allocated error of 0.08urad, 5% non-uniformity can easily meet assuming 10 urad for one pixel.

Although the pixel-to-pixel non-uniformity is an important consideration to the pointing error, with no large source of stray-light, the magnitude of error turns out to be rather small. The maximum expected error, given a 5% difference (a good detector has much better than 5%) in responsivity, is 0.23 μ rad or approximately 0.08 μ rad (1 sigma) for centroiding windows from 5x5 to 11x11 pixels.

D. Spatial Quantization

The centroiding error due to spatial quantization is caused by the finite FPA pixel size and therefore is a function of beam profile, pixel size, and centroiding window size. Unlike NEA, it is a slowly varying bias where the sub-pixel position of the beam spot determines the magnitude of the bias. Generally, centroiding window should be large to reduce spatial quantization error due to truncating the image even though this increases the NEA due to increased pixel noise. Therefore, there should always be a trade-off between these two error sources. However, we cannot increase the window size indefinitely to include the whole beam profiles due to limitations on FPA read rate. Assuming a particular beam profile (airy pattern with first minimum at 2 pixels, as shown in Fig. 5), Fig. 6 shows simulation results on spatial quantization error for centroiding window size of 7x7 pixels. This yields 1 sigma error of 0.016 urad.

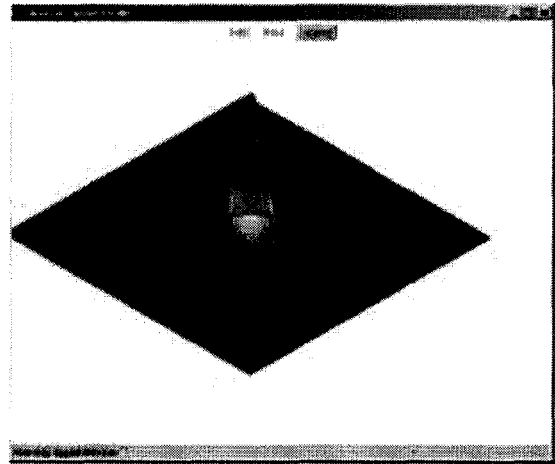


Fig. 6. Airy beam with first minimum at 2 pixels

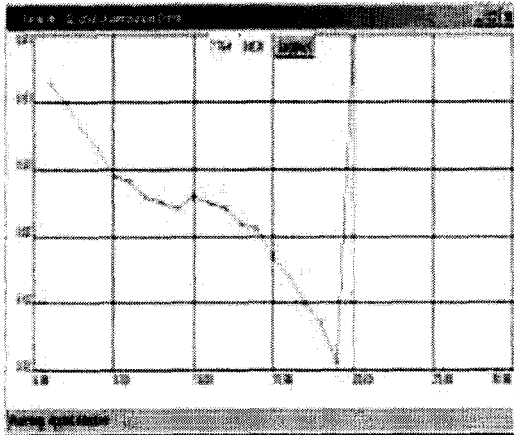


Fig. 6. The above airy beam profile can yield 1 sigma error of less than 0.02 urad.

E. Tracking Control Loop

The goal of pointing and tracking control loop is to track the beacon laser using FPA and to point downlink laser to the ground receiver using FSM. The disturbance rejection capability of the control system depends on the controller design, characteristics of FSM and time delay between control loop updates (Fig. 7). Assuming the mirror controller is optimized for the given mirror, the high FSM bandwidth and short time delay result in better rejection capability.

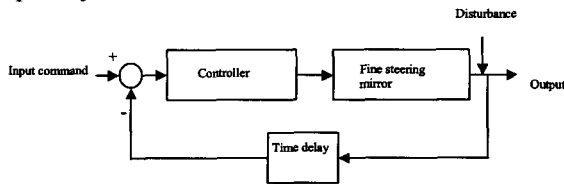


Fig. 7. Simplified block diagram of fine pointing and tracking control system.

The corresponding residual tracking error from S/C vibration PSD and tracking control disturbance rejection is calculated using equation (2).

$$\theta_{rms} = \sqrt{\int S(f) |R(f)|^2 df} \quad (2)$$

S(f): Angular S/C vibration power spectral density (PSD)
R(f): Closed loop rejection in the frequency domain

Based on the discussion above on S/C vibrations, the specified pointing error of 0.34 urad requires active vibration isolation with at least 1 kHz control update rate for vibration PSD equivalent to Olympus S/C. Gimbal vibration is treated in the same way as S/C vibration PSD. So the requirement is gimbal vibration PSD that would yield less than or equal to 0.24 urad.

Figure 8 demonstrates that using simple optical compensation only the ATP system can meet the 2 urad total pointing requirement to achieve 10 Gbps links when the platform has vibrations similar to the quiet class of S/C. In order to fly on a platform that has a noisier vibration platform passive and/or active vibration isolation would have to be introduced.

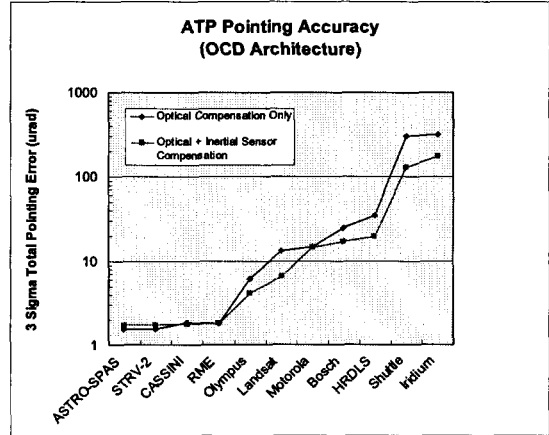


Fig. 8. Total pointing accuracy of simple optical compensation ATP Subsystem on various vibration platforms.

V. ATP LAB DEMONSTRATIONS

Beyond risk analysis, this task working on mitigating risk through a laboratory demonstration of the ATP subsystem. To this end two ATP terminals (a LEO and a GEO) have been designed and are currently being assembled. The laboratory experiment will demonstrate the ATP subsystem functionality and performance while the terminals undergo simulated spacecraft vibrations, orbital motions, and spacecraft attitude uncertainties. Fig. 9 is a cartoon of the end-end acquisition, tracking and pointing demonstration. Fig. 10 shows the assembled LEO Terminal.

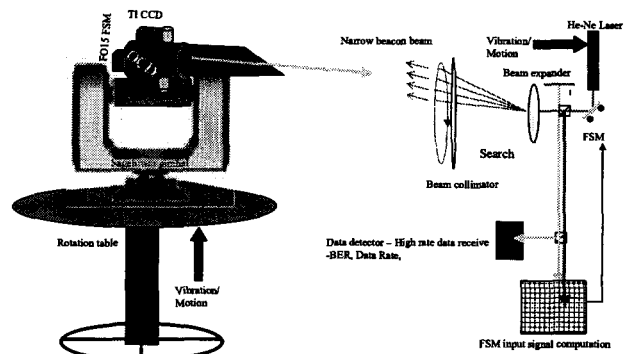


Figure 9. End-to-end LEO-to-GEO ATP Lab Demonstration.